Inward Rotating Spiral Waves in Glycolysis

Ronny Straube,[†*] Satenik Vermeer,[‡] Ernesto M. Nicola,[§] and Thomas Mair[‡]
[†]Max-Planck-Institute for Dynamics of Complex Technical Systems, Systems Biology Group, Sandtorstr. 1, Magdeburg, Germany; [‡]Biophysics Group, Institute of Experimental Physics, Otto-von-Guericke University, Universitätsplatz 2, Magdeburg, Germany; and [§]IFISC, Institute for Cross-Disciplinary Physics and Complex Systems (CSIC-UIB), Palma de Mallorca, Spain

ABSTRACT We report on the first observation of inward rotating spiral waves (antispirals) in a biochemical reaction-diffusion system. Experiments are performed with extracts from yeast cells in an open spatial reactor. By increasing the protein concentration of the extract we observe a transition from outward to inward propagating waves of glycolytic activity. Numerical simulations with an allosteric model for the phosphofructokinase can reproduce these inward propagating waves over a wide range of parameters if the octameric structure of yeast phosphofructokinase is taken into account.

Received for publication 1 March 2010 and in final form 5 April 2010.

We dedicate this work to the memory of Thomas Mair, who pioneered the study of pattern formation in allosteric enzyme systems.

*Correspondence: rstraube@mpi-magdeburg.mpg.de

Spiral-shaped concentration waves are common patterns in biological reaction-diffusion systems (1–3) which occur in both excitable and oscillatory media (4). Recently, it was shown (5–7) that oscillatory systems near a supercritical Hopf bifurcation may also support a new type of spiral wave pattern called inward rotating spiral wave or antispiral. In contrast to normal spiral waves the phase fronts of antispirals propagate toward the spiral core. The group velocity is positive for both antispirals and normal spirals, and consequently local perturbations of the wave propagate always away from the spiral core. Despite the fact that antispirals should be quite common in oscillatory media they were only observed in two chemical reaction-diffusion systems (8,9).

We report on the generation of inward propagating NADH waves in an enzyme reaction system centered on the allosteric enzyme phosphofructokinase (PFK). Glycolysis is the central metabolic pathway in virtually all organisms, and the allosteric feedback regulation of the PFK is known to be essential for the oscillatory behavior of that pathway (10–12). We have previously shown that diffusive coupling generates waves of glycolytic activity in yeast extracts (3,12,13). Here, we induce a transition from outward to inward propagating waves by increasing the protein concentration of the extract from 25 mg/ml to 60 mg/ml. In numerical simulations with the allosteric enzyme model proposed by Goldbeter (14) the antiwaves can be reproduced if the high oligomeric structure of yeast PFK is taken into account.

Experiments are performed in an open spatial reactor as described in (12). Briefly, the yeast extract, which contains the glycolytic enzymes, is fixed in a thin layer of 1.65% agarose gel. The gel is separated from a continous stirred tank reactor (CSTR) (Volume flow: 6.2 ml/h, stirring rate 500 rpm) by a cellulose triacetate membrane (MW-cut off 10 kD; Sartorius) such that the large enzymes are kept in the gel compartment whereas the metabolites and cofactors are continuously refreshed by diffusive exchange with the CSTR. Glycolytic reactions are kept in an oscillatory state by properly adjusting the inflow streams of the CSTR. The spatio-temporal dynamics of glycolytic activity were monitored via NADH fluorescence changes in the yeast extract (12).

In the range between 25 mg/ml–34 mg/ml protein concentration only outward propagating NADH waves, mostly in the form of circular-shaped waves (target patterns), are observed (Figs. 1 *A* and *C*). As the protein concentration is increased inward propagating NADH waves appeared in the range of concentrations between 40 mg/ml–60 mg/ml in eight independent experiments. In the range between 40 mg/ml–50 mg/ml, we always observed several coexisting antispirals with a wavelength larger than the system size (Movie S1 in the Supporting Material). Such a behavior is generically expected to occur close to a supercritical Hopf bifurcation or near the transition between spiral waves and antispirals where the wavelength diverges (7). At 59 mg/ml we obtained a single antispiral with a wavelength comparable to the system size (Movie S2). It was coexisting with an inward propagating circular wave (antitarget) for ~4hs (Fig. 1 *B*). During this period the spiral core exhibited a slow upward drift (Fig. 1 *D*) until it was pushed out of the observation area.

Antispiral waves are characterized by two distinct properties (5,7,8): a negative dispersion relation and an oscillation frequency ω_{AS} that is smaller than that of spatially homogeneous bulk oscillations ω_{bulk}. To confirm the latter property ($\omega_{AS} < \omega_{bulk}$) we measured the local oscillation frequency of

Editor: Alan Garfinkel.

doi: 10.1016/j.bpj.2010.04.018

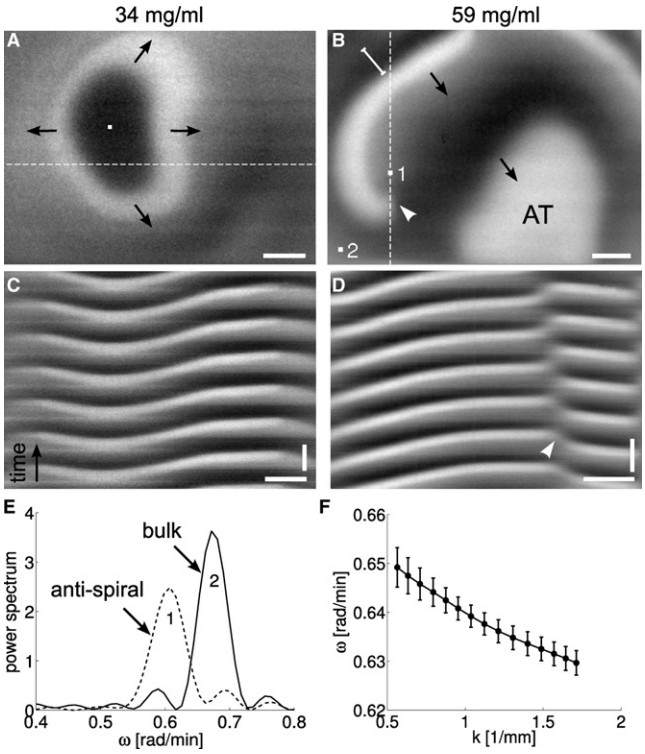

FIGURE 1 Transition from outward to inward propagating NADH waves as a function of the protein concentration of the extract. (*A*) Snapshot of an outward propagating target pattern. Local oscillation period (measured at the white dot): 12.6 min. (*B*) Snapshot of an inward rotating spiral wave and anti-target (AT). Arrows indicate the direction of wave propagation. (*C* and *D*) Space-time plots taken along the dashed lines in (*A*) and (*B*). White arrow heads in (*B*) and (*D*) mark the location of the spiral core. Scale bars: (*A* and *B*) 2mm, (*C*) and (*D*) horizontal – 2mm, vertical – 10 min. (*E*) Power spectrum of local oscillations close to the spiral core (1) and in the bulk (2) as indicated in (*B*). (*F*) Negative dispersion $d\omega/dk < 0$ measured from a one-dimensional space-time plot along the white line with bar ends shown in (*B*). Error bars are standard errors obtained from the measurement of seven subsequent wave fronts.

the NADH fluorescence close to the spiral core (Fig. 1 *B*, *region 1*) and in the lower left corner (Fig. 1 *B*, *region 2*) where bulk oscillations arrived from a region outside of the observation area. The corresponding spectra in Fig. 1 *E* show that the local oscillation frequency close to the spiral core (*dashed line*) is smaller by ~10% as compared to that of the bulk oscillations (*solid line*). This is in qualitative agreement with theoretical predictions using the complex Ginzburg-Landau equation (5,7).

The dispersion relation describes how the oscillation frequency of a wave changes with its wave number. For a spiral wave, it has to be measured in the far field where the wave front is approximately planar. Hence, we generated a one-dimensional space-time plot from a transversal intersection with the antispiral wave front in a region far away from the spiral core (cf. Fig. 1 *B*). By means of an edge-detection algorithm the wave front profiles were extracted and locally fitted by smoothing splines. From the slope of the wave front profiles we measured how the local phase velocity changes with the local oscillation period. From these two quantities we computed the local angular frequency ω and the local wave number k. The resulting dispersion curve has a negative slope (cf. Fig. 1 *F*) as expected for an antispiral (7).

To investigate the generic conditions for the occurrence of inward propagating waves in glycolysis we conducted numerical simulations using the classical Goldbeter model (14). Instead of describing the whole glycolytic pathway it focuses on the allosteric regulation of the PFK. It is assumed that the PFK comprises of n subunits to which ATP can either bind as a substrate or as an allosteric inhibitor while ADP acts as an allosteric activator of the PFK in that model. In dimensionless units it can be written as (see Supporting Material)

$$\frac{\partial}{\partial t}\alpha = \delta\nabla_{\mathbf{x}}^2\alpha + \nu - \sigma\phi_n(\alpha,\gamma) \tag{1}$$

$$\frac{\partial}{\partial t}\gamma = \nabla_{\mathbf{x}}^2\gamma + q\sigma\phi_n(\alpha,\gamma) - \gamma \tag{2}$$

where $\alpha \propto$ ATP denotes the inhibitor and $\gamma \propto$ ADP the activator. The function

$$\phi_n(\alpha,\gamma) \equiv \frac{a\alpha(1+a\alpha)^{n-1}(1+\gamma)^n}{L(1+c\alpha)^n + (1+a\alpha)^n(1+\gamma)^n} \tag{3}$$

describes the allosteric regulation of the PFK. ν and σ are proportional to the substrate influx and the PFK concentration, respectively. The parameter $\delta \equiv D_{ATP}^{eff}/D_{ADP}^{eff}$ describes a spatial scale separation. It is given by the ratio between the effective diffusion coefficients of the inhibitor and the activator. The remaining parameters c, L, a, and q were fixed at values which are compatible with experiments in well-mixed extracts (see Supporting Material) whereas σ and ν were constraint by the requirement to generate oscillatory behavior (Fig. 2 *A*).

In extensive numerical simulations we found that the number of PFK subunits n as well as the spatial scale separation δ have a significant impact on the formation of inward propagating waves (Fig. 2 *B*). Interestingly, for $\delta \leq 5$ antiwaves could not be generated for a dimeric PFK ($n = 2$) as it was used in the original Goldbeter model (14). However, when we took into account the octameric structure of yeast PFK ($n = 8$) (15) antiwaves readily appeared for a moderate spatial scale separation of $\delta \geq 1.5$ (Fig. 2 *A* and *B*). At larger values of δ antiwaves turn into stationary Turing patterns.

It is likely that in our experiments a small spatial scale separation emerges from the reversible interactions between the PFK, which is largely immobilized in the agarose gel, and its allosteric effectors (16). Since glycolytic enzymes account for at least 65% of the total amount of soluble yeast protein (17) increasing the total protein concentration of the

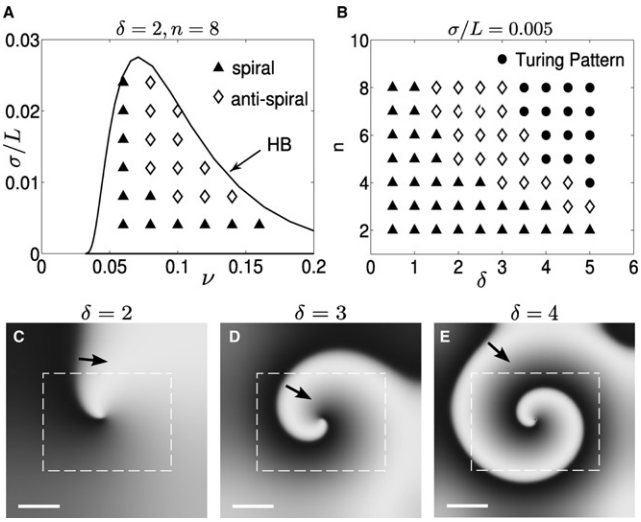

FIGURE 2 Results from numerical simulations with the Goldbeter model. (*A*) Phase diagram for the occurrence of spiral waves and antispirals as a function of the normalized PFK concentration σ and the normalized substrate influx rate ν (HB denotes a supercritical Hopf bifurcation). (*B*) Phase diagram for the occurrence of spiral waves, antispirals and Turing patterns as a function of the number of PFK subunits n and the spatial scale separation δ. For each n the value of ν was adjusted as $\nu = 0.95\nu_{H,2}(n)$ where $\nu_{H,2}(n)$ is the larger of the two Hopf bifurcation points shown in *A*. (*C*)-(*E*) Snapshots of two dimensional simulations of anti-spirals for increasing values of δ for $\nu = 0.1$ and $\sigma/L = 7 \cdot 10^{-3}$ (see Movie S3). Arrows mark the direction of wave propagation. For visual comparison with Fig. 1 *B* the experimental observation area is indicated by a dashed line. Scale bars: 5 mm. Other parameters: $L = 10^6$, $q = 5$, $c = 0$, $a = 1$.

extract (as we have done) should increase the PFK concentration in a proportional manner. A simple estimate shows that δ should increase with increasing PFK concentrations in the extract (see Supporting Material) and, therefore, favor the formation of inward propagating waves. This view is supported by the fact that the wavelength of the simulated antispirals decreased as δ was increased (Fig. 2 *C–E*). A similar scenario was also observed in the experiments where the wavelength of the antispiral waves decreased as the protein concentration of the extract was increased.

In agreement with theoretical predictions (5,6) the anti- waves arise close to the supercritical Hopf bifurcation, but could also be generated inside the oscillatory region (Fig. 2 *A*). Since the Goldbeter model is based on the quite general Monod-Wyman-Changeux mechanism (18) to describe the interaction of allosteric enzymes with their effectors, it can be expected that inward propagating waves may also occur in other diffusively coupled allosteric enzyme systems to which the Monod-Wyman-Changeux mechanism is applicable.

SUPPORTING MATERIAL

Additional text and three movies are available at http://www.biophysj.org/biophysj/supplemental/S0006-3495(10)00483-2.

ACKNOWLEDGMENTS

This work was supported by the Ministry of Education of Saxony Anhalt and the Deutsche Forschungsgemeinschaft.

REFERENCES and FOOTNOTES

1. Lechleiter, J., S. Girard, …, D. Clapham. 1991. Spiral calcium wave propagation and annihilation in *xenopus laevis* oocytes. *Nature*. 355:123–126.
2. Davidenko, J. M., A. V. Pertsov, …, J. Jalife. 1992. Stationary and drifting spiral waves of excitation in isolated cardiac muscle. *Nature*. 355:349–351.
3. Mair, T., and S. C. Müller. 1996. Traveling NADH and proton waves during oscillatory glycolysis in vitro. *J. Biol. Chem.* 271:627–630.
4. Mikhailov, A. S. 1991. Foundations of Synergetics I. Distributed Active Systems Springer, Berlin.
5. Gong, Y., and D. J. Christini. 2003. Antispiral waves in reaction-diffusion systems. *Phys. Rev. Lett.* 90:088302.
6. Brusch, L., E. M. Nicola, and M. Bär. 2004. Comment on ''Antispiral waves in reaction-diffusion systems''. *Phys. Rev. Lett.* 92. 089801, author reply 089802.
7. Nicola, E. M., L. Brusch, and M. Bär. 2004. Antispiral waves as sources in oscillatory reaction-diffusion media. *J. Phys. Chem. B*. 108: 14733–14740.
8. Vanag, V. K., and I. R. Epstein. 2001. Inwardly rotating spiral waves in a reaction-diffusion system. *Science*. 294:835–837.
9. Shao, X., Y. Wu, …, Q. Ouyang. 2008. Inward propagating chemical waves in a single-phase reaction-diffusion system. *Phys. Rev. Lett.* 100:198304.
10. Hess, B., and A. Boiteux. 1971. Oscillatory phenomena in biochemistry. *Annu. Rev. Biochem.* 40:237–258.
11. Madsen, M. F., S. Danø, and P. G. Sørensen. 2005. On the mechanisms of glycolytic oscillations in yeast. *FBES J.* 272:2648–2660.
12. Bagyan, S., T. Mair, …, S. C. Müller. 2005. Glycolytic oscillations and waves in an open spatial reactor: Impact of feedback regulation of phosphofructokinase. *Biophys. Chem.* 116:67–76.
13. Bagyan, S., T. Mair, …, R. Straube. 2008. Spatial desynchronization of glycolytic waves as revealed by Karhunen-Loeve analysis. *J. Phys. Chem. B*. 112:14334–14341.
14. Goldbeter, A., and R. Lefever. 1972. Dissipative structures for an allosteric model. Application to glycolytic oscillations. *Biophys. J.* 12: 1302–1315.
15. Kopperschläger, G., J. Bär, …, E. Hofmann. 1977. Physicochemical parameters and subunit composition of yeast phosphofructokinase. *Eur. J. Biochem.* 81:317–325.
16. Hunding, A., and P. G. Sørensen. 1988. Size adaptation of Turing prepatterns. *J. Math. Biol.* 26:27–39.
17. Hess, B., A. Boiteux, and J. Krüger. 1969. Cooperation of glycolytic enzymes. *Adv. Enzyme Regul.* 7:149–167.
18. Monod, J., J. Wyman, and J. P. Changeux. 1965. On the nature of allosteric transitions: A plausible Model. *J. Mol. Biol.* 12:88–118.

Biophysical Journal, Volume 99

Supporting Material

Inward Rotating Spiral Waves in Glycolysis

Ronny Straube, Satenik Vermeer, Ernesto M. Nicola, and Thomas Mair

Supporting Material

1 Mathematical Model

The Goldbeter model [1] is based upon the Monod-Wyman-Changeux mechanism [2] to describe the allosteric regulation of the glycolytic enzyme phosphofruktokinase (PFK), which catalyzes the conversion of fructose-6-phosphate (F6P) into fructose-1,6-bisphosphate (FBP), i.e. F6P + ATP $\rightarrow$ FBP + ADP. The model takes into account the activation of the PFK by its product ADP as well as the inhibition of the PFK by its substrate ATP. Hence, ATP and ADP play a dual role in this reaction. On the one hand, they are substrate and product of the reaction. On the other hand, they are allosteric effectors of the PFK. The unbound enzyme is supposed to have n identical subunits which perform concerted transitions between an active R and an inactive T conformation. The ratio between the forward and the backward rate defines the allosteric constant $L = k_{R\rightarrow T}/k_{T\rightarrow R}$. In addition to the substrate binding site (dissociation constant K_R) each enzyme subunit in the R state also has an activating binding site for the product ADP (dissociation constant K_P) while each subunit in the inactive T conformation has an inhibiting binding site for the substrate ATP (dissociation constant K_T). Since ATP inhibition is supposed to set in only at high ATP concentrations it generally holds that $K_T > K_R$. It is further assumed that the substrate ATP is supplied at rate ν_i while the product ADP leaves the system at rate $k_s[ADP]$.

The effective rate for the PFK catalyzed reaction is given by $nk[PFK]\bar{\phi}_n$ with

$$\bar{\phi}_n \equiv \frac{\frac{[ATP]}{K_M}\left(1+\frac{[ATP]}{K_M}\right)^{n-1}\left(1+\frac{[ADP]}{K_P}\right)^n}{L\left(1+\frac{[ATP]}{K_T}\right)^n+\left(1+\frac{[ATP]}{K_M}\right)^n\left(1+\frac{[ADP]}{K_P}\right)^n}\,. \tag{1}$$

Here, k is the intrinsic product conversion rate of a single PFK subunit and K_M denotes the Michaelis-Menten constant for a single substrate bind-

ing/product conversion step, i.e. $K_M = (k_- + k)/k_+ \equiv K_R(1 + k/k_-)$ where k_+ and k_- are the intrinsic association and dissociation rates for ATP binding as a substrate. The spatio-temporal dynamics of the PFK effectors ATP and ADP is described by the partial differential equations:

$$\begin{aligned} \frac{\partial}{\partial \bar{t}}[ATP] &= D^{eff}_{ATP}\nabla^2_{\bar{\mathbf{x}}}[ATP] + \nu_i - nk[PFK]\bar{\phi}_n \\ \frac{\partial}{\partial \bar{t}}[ADP] &= D^{eff}_{ADP}\nabla^2_{\bar{\mathbf{x}}}[ADP] + nk[PFK]\bar{\phi}_n - k_s[ADP]\,, \end{aligned} \tag{2}$$

where D^{eff}_{ATP} and D^{eff}_{ADP} denote the effective diffusion coefficients of inhibitor and activator, respectively. Eqs. 1-3 of the main text are obtained by introducing dimensionless time and spatial scales according to $\bar{t} = t/k_s$ and $\bar{x} = x(D^{eff}_{ADP}/k_s)^{1/2}$. In addition, we measure substrate and product concentrations in terms of their respective dissociation constants as $\alpha = [ATP]/K_R$ and $\gamma = [ADP]/K_P$. The dimensionless parameters in Eqs. 1-3 of the main text are then given by $\nu = \nu_i/K_R k_s$, $\sigma = nk[PFK]/K_R k_s$, $c = K_R/K_T$, $q = K_R/K_P$ and $a = K_R/K_M$.

1.1 Choice of Parameters

The constants L, k, a and K_R are fixed at the values

$$L = 10^6\,, \quad k = 500/s\,, \quad a \approx 1\,, \quad K_R = 50\mu M \tag{3}$$

in accordance with Ref. [1]. The non-exclusive binding coefficient c in Eq. 3 of the main text is typically a small number ($c \leq 0.1$), and we did not observe any noticeable effect of that parameter on anti-spiral formation in numerical simulations. Consequently, we set $c = 0$.

To obtain anti-spiral waves with a period of approximately 10 minutes (as seen in the experiments) we fixed the time scale by setting $k_s = 0.01/s$ in accordance with Ref. [3]. The spatial scale $(D^{eff}_{ADP}/k_s)^{1/2} = (D^{eff}_{ATP}/(\delta k_s))^{1/2}$ is fixed by assuming $D^{eff}_{ATP} = 10^{-6} cm^2/s$ for the effective diffusion coefficient of ATP in the agarose gel. Note that in the simulations we kept D^{eff}_{ATP} constant and varied only the ratio δ.

The dissociation constants for substrate (K_R) and product (K_P) binding to the active R conformation were reported to differ by a factor of three yielding $q = K_R/K_P = 3$, with AMP being the activator [4]. In the Goldbeter model [1] ADP has been taken as the activator which is known to be only

a weak activator for yeast PFK. Its dissociation constant lies in the same range as K_R [4] giving $q = 1$. However, for this value of q only outward propagating waves are observed in simulations. Instead, for $q \geq 3$ inward propagating waves readily appear for $\delta = 2$ and $n = 8$. This indicates that the activation of the PFK is mostly done by AMP.

The parameters σ and ν in Eqs. 1 and 2 of the main text are constrained by the requirement to generate spatially homogeneous oscillations through a supercritical Hopf bifurcation as a necessary condition to observe anti-spiral waves (see Fig. 2 of the main text).

1.2 Numerical Simulations

Two dimensional simulations were performed on a spatial grid with 176×176 grid points. Eqs. 1-3 of the main text were integrated using an explicit 4^{th}-order Runge-Kutta scheme. Since the wave length of the simulated anti-spiral waves (≥ 5 mm) is significantly larger than that of the Turing patterns (0.3-0.4 mm) we used $dt = 0.05$ and $dx = 5$ to simulate the (anti-) spiral waves and $dt = 0.01$ and $dx = 1$ to simulate the Turing patterns in Fig. 2 of the main text. To locate the border between anti-spiral waves and Turing patterns in Fig. 2B of the main text, we also performed anti-spiral simulations with $dt = 0.01$ and $dx = 1$ to confirm that the anti-spiral waves persist as the spatial step size is decreased.

2 Effective Diffusion Coefficients of ATP and ADP

In the yeast extract ATP and ADP may bind reversibly to several enzymes as allosteric effectors. If the binding affinity for the activator is larger than that for the inhibitor of the respective enzyme the effective mobility of the activator will be reduced relative to that of the inhibitor [5, 6]. For simplicity, we only estimate the change in mobility of these molecules brought about by binding to the regulatory sites of the PFK enzyme. In the presence of immobilized PFK the effective diffusion coefficients of ATP and ADP are given by [5]

$$D_{ATP}^{eff} = \frac{D_{ATP}}{1 + \frac{n[PFK]}{K_T}} \quad \text{and} \quad D_{ADP}^{eff} = \frac{D_{ADP}}{1 + \frac{n[PFK]}{K_P}}\,, \tag{4}$$

where a factor of n has been included to account for the fact that each subunit of the oligomeric enzyme can interact independently with the effector molecules. Consequently, $[PFK]$ denotes the concentration of the oligomeric PFK with n subunits. Using that $D_{ATP} \approx D_{ADP}$ and $K_T = (q/c)K_P$ we obtain for the ratio between the effective diffusion coefficients

$$\delta = \frac{D_{ATP}^{eff}}{D_{ADP}^{eff}} = \frac{1+z}{1+\frac{c}{q}z}, \quad z \equiv \frac{n[PFK]}{K_P}\,. \tag{5}$$

Since $c/q \ll 1$ the denominator is always close to one such that δ is proportional to both the PFK concentration and the number of PFK subunits.

References

[1] Goldbeter, A., and R. Lefever. 1972. Dissipative Structures for an Allosteric Model. *Biophys. J.* 12:1302–1315.

[2] Monod, J., Wyman, J., and J. P. Changeux. 1965. On the nature of allosteric transitions: A plausible Model. *J. Mol. Biol.* 12:88–118.

[3] Goldbeter, A. 1973. Patterns of Spatiotemporal Organization in an Allosteric Enzyme Model. *Proc. Natl. Acad. Sci. USA.* 70:3255–3259.

[4] Hofmann, E., and G. Kopperschläger. 1982. Phosphofructokinase from Yeast. *Methods in Enzymology.* 90:49–60.

[5] Hunding, A., and P. G. Sørensen. 1988. Size adaption of Turing prepatterns. *J. Math. Biol.* 26:27–39..

[6] Lengyel, I., and I. R. Epstein. 1992. A Chemical Approach to designing Turing patterns in reaction-diffusion systems. *Proc. Natl. Acad. Sci. USA.* 89:3977–3979.

3 Movie Captions

3.1 Movie S1

Two inward rotating spiral waves with a wave length larger than the system size. High gray values indicate a high NADH fluorescence. Protein concentration in the extract: 59mg/ml. Viewing area: 13.0mm x 9.0mm. Duration of the movie: 1850s. Local oscillation period: 612s.

3.2 Movie S2

Anti-spiral wave interacting with an anti-target. A snapshot of this movie is displayed in Fig. 1 B of the main text. High gray values denote increasing values of NADH fluorescence. Protein concentration of the extract: 59mg/ml. Viewing area: 16.7mm x 12.5mm. Duration of the movie: 1900s. Local oscillation period: 620s.

3.3 Movie 3

Numerical simulation of an anti-spiral for $\delta = 4$. A snapshot of this movie is displayed in Fig. 2 E of the main text. Shown ist the normalized concentration of ATP. Larger gray values correspond to higher concentrations. Other parameters are n=8, L=10^6, q=5, c=0, $\sigma/L = 7 \cdot 10^{-3}$ and $\nu = 0.1$. System size: 25 mm x 25 mm.